

## Pollination and Airflow Patterns Around Conifer Ovulate Cones

Karl J. Niklas and Kyaw Tha Paw U

## Pollination and Airflow Patterns Around Conifer Ovulate Cones

**Abstract.** Wind-tunnel studies indicate that the geometry of *Pinus* ovulate cones may enhance the probability of pollen entrapment by aerodynamically predetermining airflow patterns around scale-bract complexes. Pollination experiments reveal that pollen from a particular species has the highest probability of reaching the ovules of its own species. The phenomenon of species-specific pollination appears to be related to the specific morphometry of scale-bract complexes and the terminal settling velocity of pollen of the same species. These data are interpreted as evidence for a reciprocity between the aerodynamic characteristics of airborne pollen and ovulate cones of some conifer species.

Although the aerodynamic characteristics of wind-suspended pollen grains must be consistent with their entrapment by ovulate cones, the mechanics of pollen impaction are not known. Research indicates, however, that there may be a high correlation between the features which define the behavior of pollen as dispersed particles, and the morphology of ovule-bearing "cone scales" (that is, scale-bract complexes) which define close-proximity airflow patterns (1). The evidence comes from statistical analyses of the pattern and frequency of pollen impaction on the surfaces of different species of *Pinus*, as well as from wind-tunnel experiments. This report provides evidence to support the aerodynamic reciprocity hypothesis.

Freshly released pollen was collected from seven species of pine (*Pinus australis*, *P. banksiana*, *P. echinata*, *P. resinosa*, *P. rigida*, *P. strobus*, and *P. sylvestris*), discharged upwind of receptive ovulate cones at varying wind velocities, and the frequency and pattern of pollen impaction for each species was determined (2) (Table 1). For the species examined, regions of maximum pollen impaction for all orientations of the ovulate cone axis to airflow (normal, parallel, and at a 45° angle, distal end pointing downwind) were on the adaxial, proximal surfaces of scale-bract complexes. Regions of maximum pollen impacts are on the downwind surfaces of the ovulate cones when cones are oriented parallel to airflow. In normal or 45° orientations, a second region of high pollen impaction was observed on the leading surfaces of the cone. Maximum pollen impact per

scale-bract complex occurs when cones are oriented at a 45° angle to airflow (Fig. 1, A to C).

Although no correlation was found between the species of pollen that produced the maximum overall impact score and the taxonomic affinity of the ovulate cone used (Table 1), there is a distinct statistical bias of species-specific pollination ( $r = .893$ ), if only pollen impacts on the adaxial surfaces of the scale-bract complexes are compared (Table 1).

Morphometric analyses of pollen and ovulate cone features from the seven species examined indicate high intraspecific coefficients of correlation (Table 2): cone length-to-width ratio ( $r = .896$ , based on 12 individual cones from each species), number of scale-bract complexes per ovulate cone ( $r = .889$ ), pitch of the scale-bract complex parastichy ( $r = .869$ ), and scale-bract complex length-to-width and thickness-to-width ratios ( $r = .864$  and  $.895$ , respectively). Terminal settling velocities of pollen and scale-bract morphometry show a high correlation ( $r = .882$ ) for each species. The data suggest that these pollen and ovulate cone features (Table 2) may control the net deposition mechanism and explain the observed bias in pollen impaction (Table 1). Aerodynamic factors alone are not sufficient to explain the intraspecific bias (Table 1); other net deposition mechanisms such as rebound, rebound and reentrainment, or simple reentrainment may be responsible (3).

To test the aerodynamic attributes of ovulate cone morphology—specifically, the geometry of scale-bract complexes (that is, aspect ratios)—scale models of

generalized ovulate cones were constructed. These models helped in visualizing the aerodynamics of pollen entrapment. The small size of real ovulate cones, when receptive to pollination, precluded their use in wind-tunnel analyses. The characteristic air disturbance patterns created by the model were determined for different wind velocities and orientations to airflow. Airflow visualization was achieved by the bubble-streak method (4). Briefly, helium-filled bubbles (2 mm in diameter) that are neutrally buoyant (that is, the weight of the bubble is balanced by the helium), are released upwind of the model. When illuminated by an arc lamp directed toward the wind-tunnel opening, the bubbles reflect light and appear as bright streaks in photographs. Aerodynamic conformity between the models and prototype ovulate cones is ensured by the use of the appropriate Reynolds number (5). Laminar and nonlaminar airflow are shown by undisturbed and irregular bubble streaks, respectively. By correlating the airflow patterns around the model and the actual pollen impaction patterns on prototype ovulate cones, both empirical and simulated data could be used to reconstruct the aerodynamics of conifer pollination.

Regions of nonlaminar airflow statistically correlate (68 to 97 percent) with regions of high pollen impaction seen on real ovulate cones. In normal orientation, the ovulate cone model produces downwind nonlaminar flow, which causes back-sweeping eddies between and among scale-bract complexes (Fig. 1, D to F). In 45° orientation the nonlaminar flow occurs between successive scale-bract complexes (Fig. 1G). In parallel orientation, airflow eddies appear over the adaxial surfaces of each scale-bract complex (Fig. 1H). Analyses of videotapes made of nonlaminar flow around individual portions of the model indicate that air disturbance features are statistically predictable: (i) doldrum-like eddies between scale-bract complexes, (ii) corkscrew vortices around the cone axis along successive complexes, and (iii) downwind eddies that backsweep (upwind) between complexes (Fig. 1, I to J). The aspect ratios of scale-bract complexes (Table 2) provide a basis for considering complexes as airfoils which deflect suspended particles, such as pollen, toward the micropyles of attached ovules. The species-specific aspect ratios of ovulate cone scale-bract complexes together with the species-specific aerodynamic properties of pollen, such as terminal settling velocities, appear to provide some of the physical mecha-

nisms necessary to bias pollination intraspecifically. Other mechanisms, dependent on such characteristics as adhesion and surface roughness, also appear to effect the bias (3).

These studies have not been placed in

the context of larger biometeorologic systems encountered in forests or tree stands (6), nor has the influence of fascicles near ovulate cones or of clusters of ovulate cones been taken into account.

The disruption of mass airflow by

branches and leaves may decrease the relative frequency of pollen impaction, but it does not alter the potential for an intraspecific bias in pollination. The data, if verified for other pine species, support the contention that the morphol-

Table 1. Frequency (given in percentage) of pollen impaction on seven species of *Pinus* ovulate cones at the indicated settling velocity (3).

Species of ovulate cone	Pollen source and settling velocity						
	<i>P. banksiana</i> 2.0 cm/sec	<i>P. echinata</i> 2.0 cm/sec	<i>P. rigida</i> 2.1 cm/sec	<i>P. strobus</i> 2.1 cm/sec	<i>P. australis</i> 2.2 cm/sec	<i>P. resinosa</i> 2.3 cm/sec	<i>P. sylvestris</i> 2.5 cm/sec
<i>P. banksiana</i>	15 (23)*	15 (12)	16 (9)	15 (9)	15 (23)	9 (14)	15 (8)
<i>P. echinata</i>	10 (20)	14 (25)	18 (15)	19 (8)	10 (10)	20 (13)	9 (9)
<i>P. rigida</i>	17 (18)	18 (10)	23 (24)	11 (9)	11 (20)	10 (8)	10 (12)
<i>P. strobus</i>	16 (11)	10 (10)	22 (13)	15 (31)	20 (11)	9 (12)	8 (12)
<i>P. australis</i>	15 (11)	14 (9)	16 (20)	14 (9)	15 (29)	10 (12)	16 (10)
<i>P. resinosa</i>	14 (13)	9 (10)	17 (13)	13 (15)	16 (8)	17 (26)	14 (15)
<i>P. sylvestris</i>	12 (9)	10 (5)	16 (16)	16 (18)	16 (11)	17 (16)	13 (25)

\*In each entry, the first value is the percentage of pollen adhering to external surface of ovulate cone, and the value in parentheses is the percentage of pollen adhering to ovules.

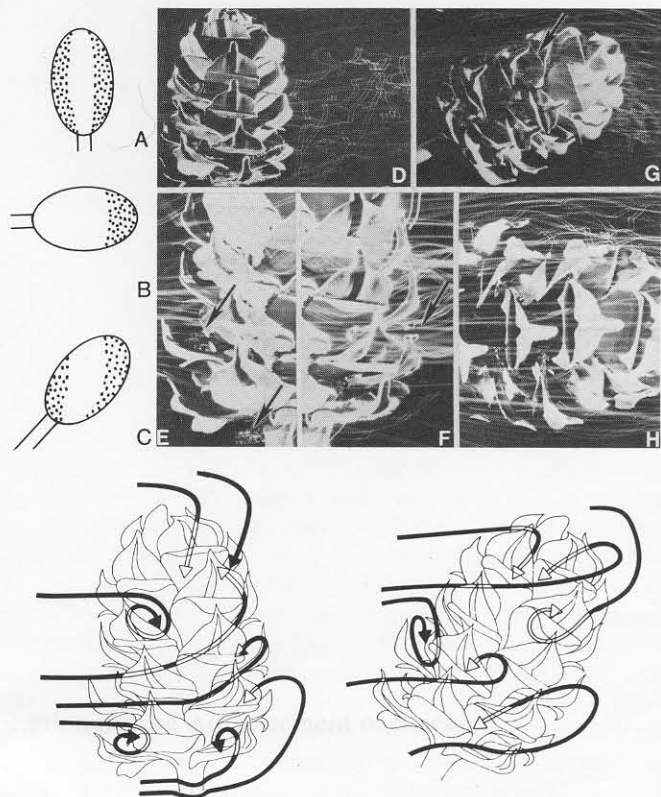
Table 2. Morphometric data of *Pinus* ovulate cones.

Species	Cone length: width*	Number of scale-bract complexes	Pitch of scale-bract genetic spiral (rad/ $\mu$ m)	Aspect ratios of scale-bract complexes		Pollen dimensions ( $\mu$ m) <sup>†</sup>	Pollen settling velocity (cm/sec)
				Length: width	Thickness: width		
<i>P. strobus</i>	2.61	74	6	4.8	0.21	34 (49) 56	2.1
<i>P. resinosa</i>	1.05	54	14	4.1	0.79	32 (52) 62	2.3
<i>P. sylvestris</i>	1.09	74	14	4.3	0.68	32 (54) 68	2.5
<i>P. banksiana</i>	1.40	48	10	3.5	0.52	31 (41) 47	2.0
<i>P. australis</i>	1.75	122	9	3.9	0.47	30 (34) 42	2.2
<i>P. rigida</i>	1.25	88	13	2.8	0.49	39 (48) 56	2.1
<i>P. echinata</i>	2.00	70	4	4.5	0.34	28 (38) 52	2.0

\*Values are based on ten sets of measurements.

<sup>†</sup>Based on 100 pollen grains: minimum (average) maximum.

Fig. 1. Empirically determined pollen impaction patterns on ovulate cone surfaces (A to C) and air disturbance patterns characteristic for an ovulate cone model (D to J) as determined by "bubble" wind-tunnel studies. Airflow in all cases is from left to right. Regions of high pollen impaction (stippled areas) are shown for ovulate cones oriented normal (A), parallel (B), and at a 45° angle (C) to airflow. (D to F) Airflow normal to the axis of a scale model of an ovulate cone shows a downwind eddy that pulses up from the lowermost scale-bract complexes (D) and down from the uppermost complexes (not shown). The downwind eddies are found in regions where pollen impaction frequencies are high (A). The upwind region of adhering pollen occurs from direct impaction. (E to F) Individual scale-bract complexes produce doldrum-like eddies (arrows) over their upper surfaces. (G) Models of ovulate cones oriented at a 45° angle to airflow produce a distal downwind eddy in a region corresponding to high pollen impaction frequencies (C). Direct impaction of pollen produces the upwind region of adhering pollen (C). (H) When oriented parallel to airflow, scale-bract complexes produce corkscrew and doldrum-like eddies. The region of maximum air disturbance occurs on the portion of the cone furthest downwind. This corresponds to the pollen impaction pattern shown in (B). (I and J) Representations of the most prevalent air disturbance patterns based on videotape analyses of cone models oriented normal (I) and at a 45° angle (J) to airflow. The ovulate cone directs unidirectional wind to vortices around and between scale-bract complexes. Impacts from pollen of the same species as the ovulate cone are found in highest frequency near or on the ovules of scale-bract complexes.



ogies of ovulate cones and pollen from the same species have responded to reproductive selective pressures incurred by anemophily. In this respect, wind pollination in the conifers appears to be a quite sophisticated and aerodynamically interactive system.

KARL J. NIKLAS

Section of Plant Biology,  
Cornell University,  
Ithaca, New York 14853

KYAW THA PAW U

Department of Agronomy,  
Purdue University,  
West Lafayette, Indiana 47907

References and Notes

1. K. J. Niklas, *Proc. Natl. Acad. Sci. U.S.A.* **79**, 570 (1982).
2. Pollen impaction patterns for each species were determined by the point discharge of about 1000 pollen grains (determined by volume) 0.5 m from the ovulate cone target at varying wind velocities (0.5 to 10 m/sec) and orientations of the cones to airflow direction (normal, parallel, and at a 45° angle to flow). The scores for each species of ovulate cone were normalized on the basis of total impact number and surface area. Counts of pollen were determined by direct microscopic observation; see also (5).
3. Species are arranged in order of increasing pollen settling velocity. If only aerodynamic mechanism were involved, deposition efficiencies would be equal for different pollen species that have the same settling velocity for a given ovule target region. It appears from the data in Table I that aerodynamic mechanisms dominate; however, *P. rigida* and *P. strobus* should have the

same percentages, but this was not observed (Table I), implying that other net deposition mechanisms are important. Theoretically, the deposition percentage on the whole cone is expected to increase with pollen of greater settling velocities (and Stokes numbers). This trend was not always apparent (Table I), indicating that nonaerodynamic mechanisms are significant in determining the observed species bias. The mechanisms involved in net deposition are impaction, rebound, rebound and reentrainment, and reentrainment, which are influenced by such factors as surface adhesion and roughness in addition to aerodynamic properties of the particles [K. T. Paw U, thesis, Yale University (1980); \_\_\_\_\_ and R. F. Reifsnnyder, in *Proceedings of the 6th Conference on Fire and Forest Meteorology*, Seattle, Washington, 22 to 24 April 1980, pp. 296-299].

4. K. J. Niklas, *Science* **211**, 275 (1981); *Am. J. Bot.* **68**, 635 (1981).
5. By means of Reynolds number ( $Re = VL\rho/\mu$ , where  $V$  is the velocity of airflow,  $L$  is a reference dimension, taken here as the length of the cone axis, and  $\rho$  and  $\mu$  are the density and viscosity of air at a given temperature), the rate of airflow within the wind tunnel was scaled to equal that of typical mass-air movement around and within conifer stands. From 0 to 10 m from the ground, airflow in conifer forests ranges from 0.5 to 2.0 m/sec; from 10 to 15 m above the ground, it ranges from 2.5 to 4.0 m/sec [R. F. Leonard and C. A. Federer, *J. Appl. Meteorol.* **12**, 302 (1973); E. R. Ford, *Agric. Meteorol.* **17**, 9 (1976); H. R. Oliver, *Q. J. R. Meteorol. Soc.* **101**, 93 (1975)].
6. R. A. Brown, G. E. McVehil, R. L. Peace, Jr., R. W. Coakley, *Cornell Aeronaut. Lab. Tech. Rep. VT-2408-1* (1969); E. J. Plate and A. A. Ouraishi, *J. Appl. Meteorol.* **4**, 400 (1965); I. A. Singer and M. E. Smith, *J. Meteorol.* **10**, 121 (1953).
7. K. J. Niklas and K. T. Paw U, unpublished observations.
8. Supported by NSF grant DEB-81-18749

26 February 1982; revised 5 May 1982

